Hindawi
Advances in Civil Engineering
Volume 2020, Article ID 6625132, 10 pages
https://doi.org/10.1155/2020/6625132

Research Article

Calculation of Soil Deformation Caused by Shield Tunneling through the Sludge Layer with Plastic Drainage Plates

Fan Zhang,[1] **Linchong Huang**,[2] **and Yu Liang**[2]

[1]*School of Intelligent Systems Engineering, Sun Yat-Sen University, Shenzhen 518000, China*
[2]*School of Aeronautics and Astronautics, Sun Yat-Sen University, Shenzhen 518000, China*

Correspondence should be addressed to Yu Liang; liangyu25@mail.sysu.edu.cn

Received 9 October 2020; Revised 9 November 2020; Accepted 10 November 2020; Published 30 November 2020

Academic Editor: Mingfeng Lei

Due to a lack of engineering experience, research on ground deformation during shield machine tunneling in sludge layers is limited, especially in areas with plastic drainage plates installed for ground stabilization. When the shield passes through this area, the shield cutterhead may be jammed by the drainage plates, resulting in excavation surface instability, excess ground deformation, and schedule delay. In this work, a Mindlin solution for ground deformation in such a layer is obtained, considering four factors: the frontal additional pressure generated by the shield cutterhead due to the soil squeezing effect, the uneven lateral friction between the shield shell and the soil, the frontal friction generated by the shield cutterhead when cutting through the drainage plate, and the shield machine restart after shutdown. The results show that the theoretical curve is in good agreement with the measured values. The maximum settlement was approximately 10 m behind the excavation surface, and the maximum uplift was approximately 5 m in front of the excavation surface. The most influential factor among all the studied factors was the additional pressure on the shield cutter, which accounted for approximately 56% of the maximum settlement and 60% of the maximum uplift. The soil settlement mainly occurred within 12 m on both sides of the tunnel axis. The maximum settlements at the different soil depths tested were all directly below the tunnel axis.

1. Introduction

With the development of urban construction in China, various types of municipal projects, such as subways, cross-river tunnels, sewage pipes, and utility tunnels, have been carried out. Pipe jacking and shield tunneling are the two most common construction methods. Due to a lack of engineering experience, research on ground deformation during pipe jacking shield tunneling in sludge layers is limited, especially when the layer is installed with plastic drainage plates for ground stabilization.

The calculation methods used to determine the soil deformation caused by shield machines include the empirical formula analysis, theoretical analysis, numerical analysis, and model testing. Based on the analysis of a large number of field monitoring data, Peck proposed the calculation formula of surface settlement prediction [1]. Later, many scholars developed different empirical solutions according to different stratigraphic conditions on the basis of this formula [2–4].

The development of the finite element method has shifted from simple stress field simulation to multifield coupled simulation [5–9]. Model tests can be used to simulate formation deformation during the tunneling process on a small scale [10–13], with the disadvantages of high cost and low adaptability.

Due to its rigorous framework, theoretical analysis has been widely used. Sagaseta [14] proposed a method to estimate surface settlements by using the ground volume loss parameter. Verruijt and Booker [15] considered the elliptic deformation of the surrounding ground and proposed a solution for tunneling-induced ground surface settlements. Loganathan and Poulos [16] proposed the concept of equivalent ground loss parameters. The random medium

method is also one of the commonly used methods for formation disturbance [17–19]. These theoretical methods have inspired a series of follow-up studies [20–27].

Some scholars [28–35] have considered the impact of multiple factors, such as additional thrust Q, frontal friction force f_d on the cutter plate, lateral friction f_s on the shield shell, and grouting pressure P, on surface settlement based on the Mindlin solution. The existing research results show that these three factors, the frontal additional pressure generated by the shield cutterhead, the uneven lateral friction between the shield shell and the soil, and the frontal friction, are the main causes of formation deformation during tunneling. Therefore, the above three factors are essential for the theoretical analysis method proposed in this paper.

However, these studies did not take into account the impact of machine restart on the soil layer displacement after machine shutdown or the impact when the shield passes through special layers, such as sludge layers installed with plastic drainage plates. This paper innovatively considers the influence of shield machine restart after shutdown on soil deformation.

Based on the Mindlin solution, four factors that affected formation deformation during shield tunneling were considered in this paper: the frontal additional pressure generated by the shield cutterhead due to the soil squeezing effect, the uneven lateral friction between the shield shell and the soil, the frontal friction generated by the shield cutterhead when cutting through the drainage plate, and the shield machine restart after shutdown. Then, the formula for calculating the vertical displacement of a stratum during construction was obtained. Finally, based on a project case, the calculated value and the measured result were compared and analyzed to verify the rationality of the calculation method proposed above.

2. Assumptions

Complex mechanical behavior occurs during shield tunneling. The following assumptions are made:

(1) The soil is undrained, consolidated, homogeneous, linear elastic, and semi-infinite; only the deformation caused by construction is considered.

(2) The shield remains horizontal during the tunneling process.

(3) The friction force between the shield and the surrounding soil is unevenly distributed, and the additional thrust on the front is distributed evenly.

3. Calculation of Soil Displacement Caused by Shield Tunneling

3.1. Mindlin Solution. Based on Galerkin's solution, Mindlin [36] deduced the formula for the displacement at any point in an elastic half-space. A force is applied at point p (0, 0, c) and acts in the positive z or x direction (see Figure 1).

The vertical displacement w_v and horizontal displacement v_v at any point in the soil caused by the vertical concentrated force P_v can be written as

$$w_v = \frac{P_v}{16\pi G(1-\nu)}\left[\frac{3-4\nu}{R_1} + \frac{8(1-\mu)^2-(3-4\mu)}{R_2} + \frac{(z-c)^2}{R_1^3} + \frac{(3-4\mu)(z'+c)^2 - 2cz'}{R_2^3} + \frac{6cz'(z'+c)^2}{R_2^5}\right], \tag{1}$$

$$v_v = \frac{P_v\sqrt{x'^2+y'^2}\cos\varphi}{16\pi G(1-\mu)}\left[\frac{z'-c}{R_1^3} + \frac{(3-4\mu)(z'-c)}{R_2^3} + \frac{4(1-\mu)(1-2\mu)}{R_2(R_2+z'+c)} + \frac{6cz'(z'+c)}{R_2^5}\right]. \tag{2}$$

The vertical displacement w_h, horizontal displacement v_h, and longitudinal displacement u_h at any point in the soil caused by the horizontal concentrated force P_h in the elastic half-space can be expressed as

$$w_h = \frac{P_h x'}{16\pi G(1-\mu)}\left[\frac{z-c}{R_1^3} + \frac{(3-4\mu)(z'-c)}{R_2^3} - \frac{6cz'(z'+c)}{R_2^5} + \frac{4(1-\mu)(1-2\mu)}{R_2(R_2+z'+c)}\right],$$

$$v_h = \frac{P_h x' y'}{16\pi G(1-\mu)}\left[\frac{1}{R_1^3} + \frac{(3-4\mu)}{R_2^3} - \frac{6cz'}{R_2^3} - \frac{4(1-\mu)(1-2\mu)}{R_2(R_2+z'+c)^2}\right], \tag{3}$$

$$u_v = \frac{P_h}{16\pi G(1-\mu)}\left[\frac{3-4\mu}{R_1} + \frac{1}{R_2} + \frac{x'^2}{R_1^3} + \frac{(3-4\mu)x'^2}{R_2^3} + \frac{2cz'}{R_2^3}\left(1-\frac{3x'^2}{R_2^2}\right) + \frac{4(1-\mu)(1-2\mu)}{R_2+z'+c}\left[1-\frac{x'^2}{R_2(R_2+z'+c)}\right]\right],$$

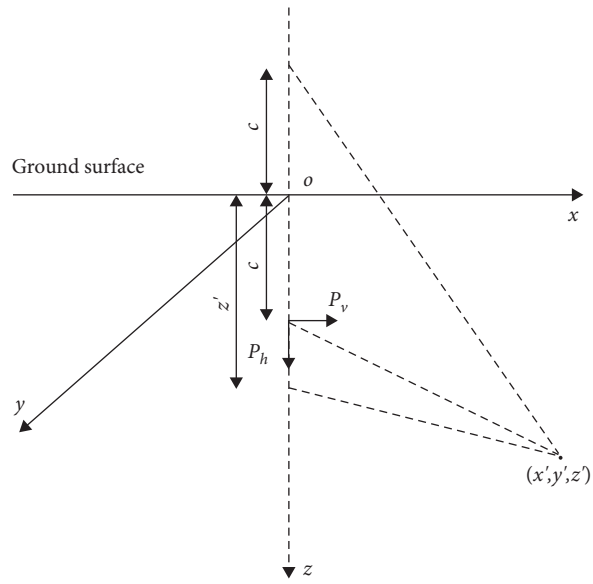

Figure 1: A schematic diagram of the Mindlin solution calculation.

where μ is Poisson's ratio, G is the shear modulus, and R_1, R_2, and ϕ can be written as

$$R_1 = \sqrt{x'^2 + y'^2 + (z' - c)^2},$$
$$R_2 = \sqrt{x'^2 + y'^2 + (z' + c)^2}, \quad (4)$$
$$\varphi = \sin^{-1}\frac{y'}{\sqrt{x'^2 + y'^2}}.$$

3.2. Vertical Displacement Caused by the Frontal Additional Pressure. The frontal additional pressure was divided into two parts: the pressure caused by the rotation of the cutterhead and the extrusion pressure caused by the cutting into the soil. The effect of the frontal additional pressure at the tunnel face can be analyzed by evaluating the displacement field in the half-space subjected to concentrated force. The vertical displacement w_{1q} and horizontal displacement v_{1q} of the stratum caused by the frontal additional pressure can be obtained by integrating equation (1).

The global coordinate system is the orthogonal coordinate system, while the local coordinate system is the polar coordinate system. At this point, the coordinate transformation relationship is defined as $m = 0$, $n = r\cos\theta$, and $c = H - r\sin\theta$. As shown in Figure 2, the integral variable is $rdrd\theta$. The formulas for both vertical and horizontal displacements of the stratum caused by the frontal additional pressure can be given as follows:

$$w_{1q} = \int_0^R \int_0^{2\pi} qr\mathrm{d}r\mathrm{d}\theta \frac{x}{16\pi G(1-\mu)}\left[\frac{z - H + r\sin\theta}{R_1^3} + \frac{(3-4\mu)(z - H + r\sin\theta)}{R_2^3}\right.$$
$$\left. - \frac{6(H - r\sin\theta)z(z + H - r\sin\theta)}{R_2^5} + \frac{4(1-\mu)(1-2\mu)}{R_2(R_2 + z + H - r\sin\theta)}\right],$$
$$v_{1q} = \int_0^R \int_0^{2\pi} qr\mathrm{d}r\mathrm{d}\theta \frac{x(y - r\sin\theta)}{16\pi G(1-\mu)}\left[\frac{1}{R_1^3} + \frac{3-4\mu}{R_2^3} - \frac{6(H - r\sin\theta)z}{R_2^5} + \frac{4(1-\mu)(1-2\mu)}{R_2(R_2 + z + H - r\sin\theta)^2}\right], \quad (5)$$
$$R_1 = \sqrt{x^2 + (y - r\cos\theta)^2 + (z - H + r\sin\theta)^2},$$
$$R_2 = \sqrt{x^2 + (y - r\cos\theta)^2 + (z + H - r\sin\theta)^2}.$$

3.3. Vertical Displacement Caused by Uneven Lateral Friction. Based on a previous study, the total friction was mainly composed of the following items: lateral friction between the shield shell and the surrounding soil and frontal friction of the shield cutter head. The analytical solutions of the additional stresses caused by these two frictional forces were

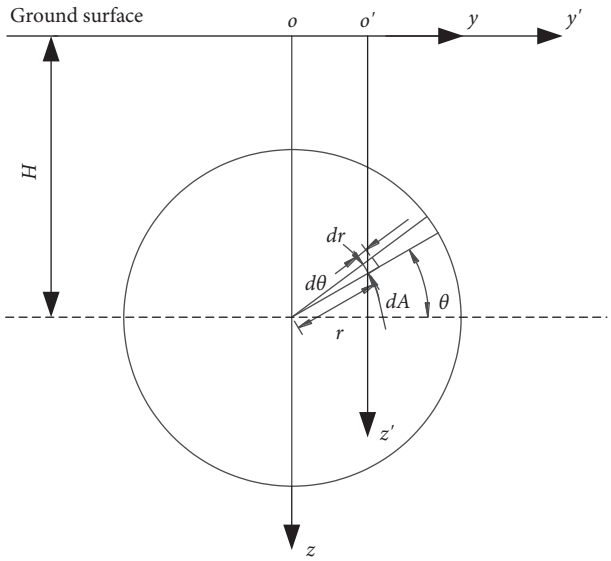

Figure 2: Integral diagram of the additional thrust on the front of the shield machine.

derived. The ground settlement caused by friction between the shield shell and soil was increased due to the shield machine restarting after a long shutdown. The lubrication effect of grouting was poor when it was restarted.

The settlement affected by the long-term shutdown and restart factors was much larger than that in the normal situation because during the shutdown process, the strength of the disturbed soil was restored, leading to a significant increase in friction between the shield and the soil [28]. The formula for calculating the shear force between the pile and the soil was derived by *E.* Alonso et al. [37]. When this formula is applied to the friction between the shield machine and the soil layer, the formula for the friction in any α position on the outer wall of the shield machine can be given as

$$f = \tau_{sr} = \beta_s \sigma'_\alpha \tan \delta', \tag{6}$$

where σ'_α is the radial normal stress on the shell of the shield machine, which is defined as follows:

$$\begin{aligned} \sigma'_\alpha &= \sigma'_v \sin^2 \theta + \sigma'_h \cos^2 \theta, \\ \sigma'_v &= \sigma_{axis}{}' - \gamma R \sin \theta, \\ \sigma'_h &= K_0 \sigma'_v, \end{aligned} \tag{7}$$

where σ'_v is the vertical component force; σ'_h is the horizontal component force; $\sigma_{\text{axis}}{}'$ is the vertical earth pressure at the position of the tunnel axis (kPa); and K_0 is the lateral static earth pressure coefficient. δ' is the friction angle of the contact surface between the shield machine and the soil. The friction angle of the contact interface between steel and clay ranges from 6.5° to 9°.

By integrating the vertical displacement formula for any point at which displacement was caused by the horizontal concentrated force in the Mindlin solution (see Figure 3), the displacement caused by the uneven lateral friction between the shield shell and the soil can be obtained:

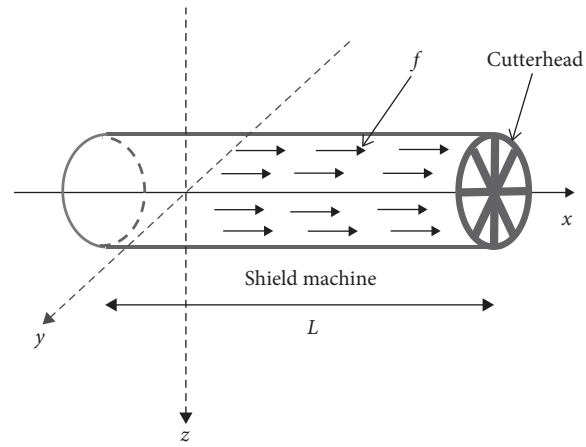

Figure 3: Calculation model of soil deformation caused by uneven lateral friction.

$$\begin{aligned} w_{2f} = \int_0^{2\pi} \int_0^L \frac{f R dl d\theta (x+l)}{16\pi G(1-\mu)} \Big[& \frac{z - H + R\sin\theta}{R_3^3} \\ & + \frac{(3-4\mu)(z - H + R\sin\theta)}{R_4^3} \\ & - \frac{6(H - R\sin\theta) z (z + H - R\sin\theta)}{R_4^5} \\ & + \frac{4(1-\mu)(1-2\mu)}{R_4 (R_4 + z + H - R\sin\theta)} \Big], \end{aligned} \tag{8}$$

where L is the length of the shield machine (m) and R_3 and R_4 can be given as

$$\begin{aligned} R_3 &= \sqrt{(x+l)^2 + (y - R\cos\theta)^2 + (z - H + R\sin\theta)^2}, \\ R_4 &= \sqrt{(x+l)^2 + (y - R\cos\theta)^2 + (z + H - R\sin\theta)^2}. \end{aligned} \tag{9}$$

3.4. Vertical Displacement Caused by Frontal Friction at the Shield Cutterhead. In practical engineering, plastic drainage plates are usually used to reinforce ground foundations. For this work, the polyethylene plastic drainage plate has a tear strength of 20 kN, width of 100 mm, and thickness of 4 and 5 mm. When the shield passes through the reinforced area, the plastic drainage plates will be cut by the shield cutter, and the cutterhead may be jammed by them. Therefore, the friction at the front surface of the shield will also increase.

Figure 4 shows the calculation model of soil deformation caused by the frontal friction at the shield cutterhead. A model of additional stress considering the effect of friction was established. Suppose that the total number of cutting wheel spokes in the cutterhead is n and that the stress on the spokes has a triangular distribution.

In the coordinate system shown in Figure 4, the cutterhead is located in the yz plane, while the concentrated load is located in the xz plane. The coordinate transformation relationship is defined as $x = -y'$, $y = x'$, and $z = z'$.

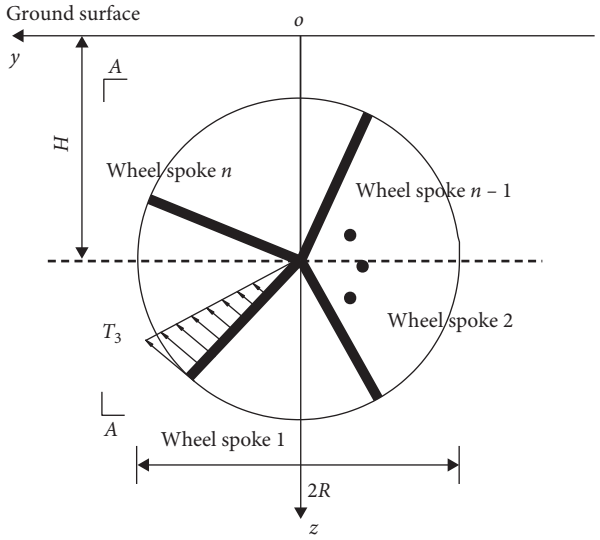

Figure 4: Calculation model of soil deformation caused by frontal friction of the shield machine cutter head.

The very small area $r\mathrm{d}r$ is on the front side of the shield cutter. The friction between the cutter head and the soil was decomposed to obtain the horizontal and vertical components. The surface deformation caused by the friction between the front of the shield cutter and the soil layer was obtained:

$$w_{3f} = \sum_{n=1}^{m} \int_0^R \left\{ \frac{p_1 \cos\phi}{\pi G} \left[\frac{2(1-\nu)R_5^2 + (H + r\sin\phi)^2}{R_5^3} \right] - \frac{p_1 \sin\phi (y - r\cos\phi)}{\pi G} \cdot \left[\frac{-H - r\sin\phi}{R_5^3} + \frac{1-2\nu}{R_5 (R_5 + H + r\sin\phi)} \right] \right\} r\mathrm{d}r,$$

$$p_1 = \frac{2(T_1 + T_3)}{(nR^2)}, \tag{10}$$

where p_1 is the maximum torque by each spoke; T_1 is the frontal friction of the cutterhead; T_3 is the cutting torque of the cutterhead; y is the horizontal distance between the calculated point and the tunnel axis; m is the total number of spokes on the cutterhead, $n = 1, 2, 3, \ldots, m$; ϕ is the initial angle of the tool; R is the outside radius in the shield machine; and H is the burial depth of the tunnel axis,

$$R_5 = \sqrt{x^2 + (y - r\cos\phi)^2 + (H + r\sin\phi)^2},$$
$$\phi = \varphi + \frac{2\pi(n-1)}{m}. \tag{11}$$

3.5. Vertical Displacement Caused by Restarting After Shutdown. During the tunneling process, the shield machine is usually restarted after shutdown. Shutdown usually occurs for maintenance or other technical reasons. During a long shutdown, the slurry circulation is stopped, and the lubrication effect of the slurry is greatly reduced. Even the grout behind the shield shell will solidify. The total thrust of the Jack greatly increases when the shield machine restarts. Thus, a large settlement will occur by restarting after shutdown.

The existing analytical models do not consider the influence of shield machine restarting after shutdown. The frequent shutdown of the shield machines when cutting the plastic drainage plate was considered in this work. Through onsite monitoring of jacking force data, the impact of shutdown can be inferred:

$$F = P_A + P_\mathrm{f} + T,$$

$$P_A = \left\{ \left[\gamma \cdot (H - H_\mathrm{w}) + \gamma' \cdot H_\mathrm{w} \right] \cdot K_a - 2c \cdot \sqrt{K_a} \right\} \cdot \frac{\pi D^2}{4}. \tag{12}$$

F refers to the total thrust; P_A refers to the positive resistance during jacking; P_f refers to the side resistance during jacking; c is the soil cohesion, kPa; γ is the soil weight, kN/m^3; γ_w is the water weight, taken as 10 kN/m^3; γ' was the soil saturation weight, kN/m^3; K_a is the active Earth pressure coefficient,

$$K_a = \tan^2\left(\frac{\pi}{4} - \frac{\phi}{2}\right). \tag{13}$$

The side resistance during jacking was calculated. The field monitoring data of total Jack forces F are shown in Figure 5.

3.6. Total Displacement Caused by Multiple Factors. Based on the analysis mentioned above, four factors were considered in this work: the frontal additional pressure generated by the shield cutterhead, the uneven lateral friction between the shield shell and the soil, the frontal friction generated by the shield cutterhead when cutting through the drainage plate, and the shield machine restart after shutdown. The total vertical displacement of the formation induced by shield tunneling can be obtained by superimposing all the components mentioned above:

$$w = w_{1q} + w_{2f} + w_{3f} + w_T, \tag{14}$$

where w_{1q} is the vertical displacement of the soil induced by additional thrust on the front of the shield, w_{2f} is the vertical displacement of the soil induced by uneven friction on the side of the shield machine, w_{3f} is the vertical displacement of the soil induced by frontal friction of the shield machine cutterhead, and w_T is the vertical displacement of soil induced by restarting after shutdown.

3.7. Project Case. A shield-driven power pipe gallery in Guangzhou was analyzed in this work. The selected interval started from $K0 + 000$~$K5 + 581.9$, with a total length of 5581.9 m, and 13 wells (6 working wells and 7 receiving

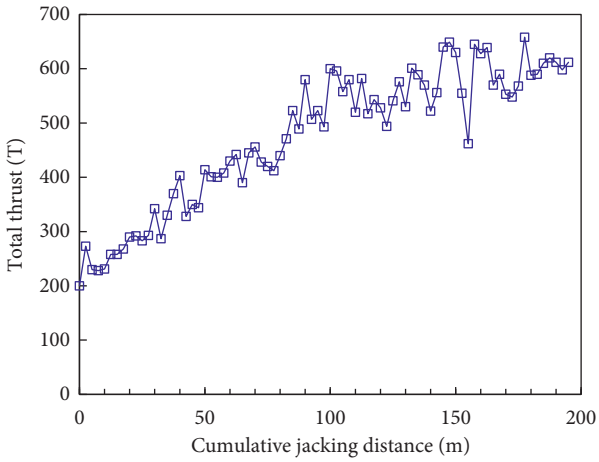

Figure 5: Curve of total thrust with mileage.

wells) were adopted. The outer diameter of the tunnel was 3.6 m, and the cover depth was 4.75~13.59 m, with a maximum longitudinal slope of 1.72% (intervals #12-11). The slurry-water balanced shield machine was used for excavation.

The crossing strata in this interval were mainly silt. An existing municipal road passes through this section, and the foundation under the road surface was reinforced with plastic drainage plates (see Figure 6). When the shield passes through the reinforced area, the plastic drainage plates will be cut by the shield cutter, and the cutter head could be jammed by them. The tunneling risk was thus increased by the presence of the plastic drainage plates, and there were multiple shutdown accidents during the tunneling process of this section.

3.8. Selection of Analysis Parameters. The main calculation parameters were as follows: overlay thickness $H = 9$ m; average soil weight $\gamma = 16.22$ kN/m^3; filling layer $h_1 = 2$ m, $\gamma_1 = 16$ kN/m^3; silt layer $h_2 = 5$ m, $\gamma_2 = 16$ kN/m^3; silty clay layer $h_3 = 2$ m, $\gamma_3 = 17$ kN/m^3; $q = 20$ kPa; Poisson's ratio of the soil $\mu = 0.42$; compression modulus of the soil $E_s = 4$ MPa; vertical Earth pressure at the position of the tunnel axis $\sigma_{\text{axis}}{}' = 146$ kPa; soil shear modulus $G = 225$ kPa; coefficient of lateral static earth pressure $k_0 = 0.6$; pipe jacking head length $L = 6$ m; friction angle of the contact surface between the shield shell and the soil was $\delta' = 8^\circ$; number of cutter spokes $m = 8$; shield machine outer diameter 3.6 m; shield machine inner diameter 3 m; cutterhead radius 1.8 m; initial cutter angle $\phi = 15^\circ$.

3.9. Ground Surface Displacement. The above parameters were substituted into equation (14) for calculation, the curves of ground deformation caused by various influencing factors were obtained, and the results are presented in Figure 7.

When the plastic drain plate was cut by the cutterhead of the shield, the impact of the frontal friction of the cutterhead increased. This result was the same as the increase in the cutter head frontal friction T_1 and cutting torque T_3:

Figure 6: Plastic drainage plate layout.

$$T_1 = \frac{2\pi(1-k)\mu' R^3 P'}{3}, \tag{15}$$

where μ' is the friction coefficient between the cutter head and the plastic drain plate in the soil layer, which is set to 0.4, and k is the cutter opening rate, which is set to 35%. P' refers to the horizontal earth pressure in the center of the cutterhead, which was taken as 0.1 MPa according to site data. Finally, $T_1 = 317.26$ kNm:

$$T_3 = m_1 F_r R_d + m_2 F_c R_c, \tag{16}$$

where m_1 is the number of spokes; F_r is the rolling force of the cutterhead spoke; R_d is the average turning radius of the cutterhead spokes, m; m_2 is the number of cutters; F_c is the cutting resistance of a single cutter, kN; and R_c is the average radius of cutter position, m. The cutterhead was equipped with a shell knife, center fishtail knife, scraper, and tearing knife, which worked together to effectively cut the plastic drainage plate in the soil layer. Therefore, it was assumed that the torque of cutting the soil was $T_3 = 800$ kNm. The parameters were substituted into the previously presented formula, which was calculated by MATLAB.

Figure 8 shows the longitudinal profiles of displacement due to different factors. The ground surface first uplifted ahead of the tunnel face and then subsided behind it. The tendency of ground deformation caused by the two factors was as follows: the front thrust of the shield machines and the uneven friction on the shield shell were similar. However, the ground deformation caused by restarting after a shutdown exhibited the opposite trend compared with the previous two factors. The vertical displacement of the ground caused by the frontal friction appeared as an uplift trend and was mirror-symmetric about the excavation surface along the tunneling direction. As shown in Figure 8, the maximum settlement was located approximately 10 m behind the excavation surface, and the maximum settlement was approximately 4 mm; the maximum uplift was located approximately 5 m in front of the excavation surface, and the maximum was approximately 7.5 mm.

During the shield tunneling process, the vertical settlement of the ground surface was caused by four factors: the frontal additional pressure generated by the shield cutterhead due to the soil squeezing effect, the uneven lateral friction

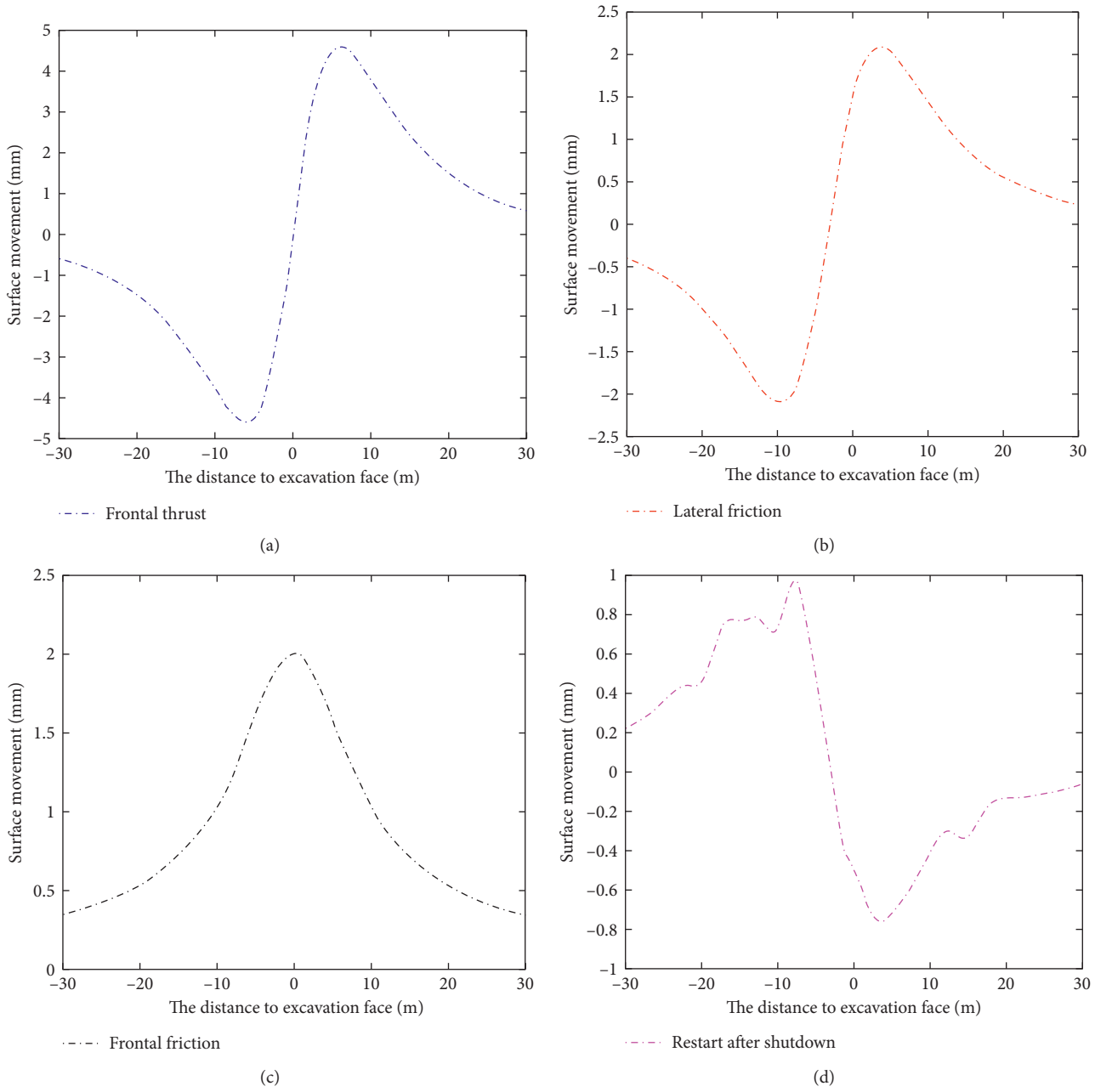

Figure 7: Surface deformation curves caused by various factors, (a) frontal additional pressure, (b) uneven lateral friction, (c) frontal friction generated by the shield cutterhead, and (d) shield machine restart after shutdown.

between the shield shell and the soil, the frontal friction generated by the shield cutterhead when cutting through the drainage plate, and the shield machine restart after shutdown. The biggest influencing factor was the frontal additional pressure generated by the shield cutterhead due to the soil squeezing effect. When the total settlement reached the maximum value, the surface settlement caused by the frontal additional pressure was 5 mm, which accounted for approximately 56% of the total ground settlement; the uneven lateral friction between the shield shell and the soil resulted in a surface settlement of 2 mm, accounting for approximately 22%; the vertical deformation of the ground caused by the friction at the front of the shield machine and the restart factor after shutdown were manifested as uplift, both accounting for approximately 11% of the total settlement.

The biggest influencing factor for surface uplift deformation was also the frontal additional pressure. When the total uplift of the local surface reached the maximum value, the surface uplift caused by the additional thrust was 4.5 mm, accounting for approximately 60% of the total ground uplift. The uneven lateral friction, which resulted in a ground surface uplift of 2 mm, accounted for approximately 27% of the total ground uplift. The third influencing factor was the friction at the front of the shield machine, which resulted in a

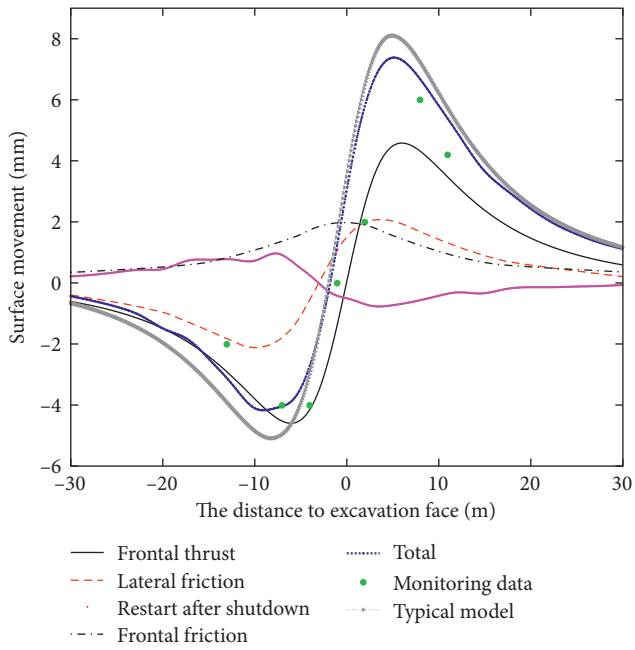

Figure 8: Longitudinal profiles of displacement due to different factors.

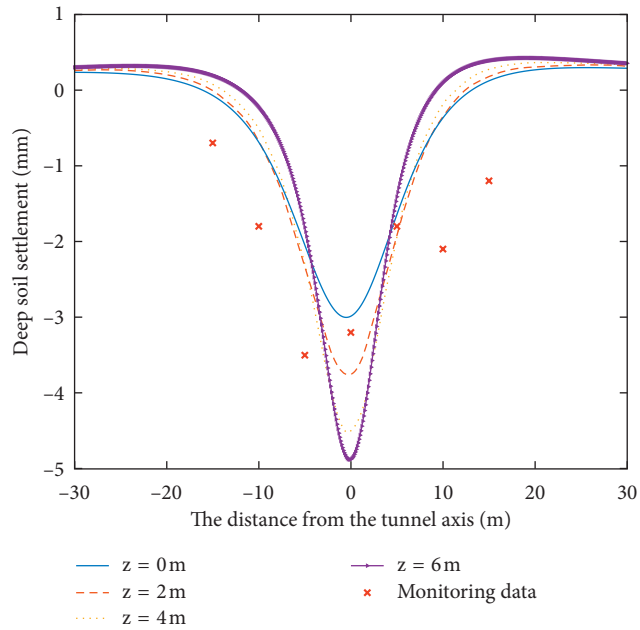

Figure 9: Lateral soil settlement curves at different depths ($x = -4$ m).

surface uplift of 1.5 mm, accounting for approximately 20% of the total ground uplift. The vertical deformation caused by the restart factor after shutdown was manifested as settlement. The settlement magnitude was 1 mm (the uplift value was −1 mm), so it was approximately −7% of the total uplift.

The calculated value was consistent with the monitored data. The monitored maximum ground surface settlement was 4.5 mm, which was 11% more than the results obtained by the proposed method. The monitored maximum ground surface uplift was 6.5 mm, which was 13% less than the results obtained by the proposed method. The difference between the monitored data and the calculated data mainly comes from two aspects: (a) it was assumed that the foundation is a homogeneous elastic foundation model, but in fact, the properties of the soil varied with depth. (b) The settlement of underground soil was difficult to observe. During the process of installing the sensor and reading the data, the soil structure may have changed. Although there was a divergence between the two methods, the proposed method provided a relatively satisfactory estimation of the ground deformation profile, and the calculation efficiency was very high.

The curves for the theoretical model proposed in this paper, the typical model curve, and monitoring data are shown in Figure 8. The ground surface settlement and uplift obtained from the typical model are relatively large, and the curves for the theoretical model proposed in this paper is in good agreement with the field measurements, meaning that the ground surfaces settlement caused by the shield construction can be predicted more accurately.

3.10. Deep Soil Settlement. By changing the calculated depth of the soil, an analysis of the deep soil settlement was performed by assuming that $z = 0$, 2, 4, or 6 m, while the other parameters remained unchanged. A cross section (4 m behind the excavation face) was selected, and the soil settlement at different depths during excavation was calculated and compared with the measured data onsite, as shown in Figure 9.

As seen from Figure 9, the lateral soil settlement at different depths of the soil layer was mainly concentrated within a range of approximately 12 m from the tunnel axis. The curve was an approximately normal distribution curve. As the depth of the soil layer increased, the maximum soil settlement gradually increased, and the maximum soil settlement was located directly below the tunnel axis. However, with increasing distance from the tunnel axis, the settlement did not increase with depth. Instead, it reversed at a distance 4–6 m from the axis, after which the settlement decreased with increasing depth. The curve obtained by the calculation was basically consistent with the field monitoring data, yet the calculated values plotted lower than the monitored one. The monitored maximum settlement was 3.7 mm, which appeared approximately 3 m behind the excavation face. The calculated settlement was 2.8 mm, and the error was approximately 24%. The reason for the error was that the effect of grouting pressure and formation loss on the surface settlement was not considered in the deformation analysis.

4. Conclusions

Based on a power pipe gallery project, four factors resulting in stratum deformation were analyzed: the frontal additional pressure generated by the shield cutterhead due to the soil squeezing effect, the uneven lateral friction between the shield shell and the soil, the frontal friction generated by the shield cutterhead when cutting through the drainage plate, and the shield machine restart after shutdown. The following conclusions were drawn from this work:

(1) The ground settlement curve considering multiple factors was in good agreement with the measured values. The calculation result could reflect the longitudinal surface settlement during the tunneling process. The ground surface first uplifted ahead of the tunnel face and then subsided behind it. The maximum settlement was located approximately 10 m behind the excavation surface and was approximately 4 mm; the maximum uplift was located approximately 5 m in front of the excavation surface and was approximately 8 mm.

(2) Among the four factors mentioned above, the most influencing factor of ground deformation was the frontal additional pressure generated by the shield cutterhead due to the soil squeezing effect. It accounted for 56% of the maximum settlement and approximately 60% of the maximum uplift deformation.

(3) A section behind the excavation surface was selected to analyze and compare the soil settlement at different depths. The settlement mainly appeared within 12 m on both sides of the tunnel axis, and the curve approximately obeyed the normal distribution. The maximum settlements at different soil depths were directly below the tunnel axis. With the increase in the distance from the tunnel axis, the curve no longer conformed to the law that the settlement value increases with depth. Instead, it reversed at a distance 4–6 m from the axis, and then the settlement decreased with increasing depth.

Data Availability

The data used to support the findings of this study are available from the corresponding author upon request.

Conflicts of Interest

The authors declare that there are no conflicts of interest regarding the publication of this paper.

Acknowledgments

This work was sponsored by the National Natural Science Foundation of China, China (nos. 51708564, 51678578, and 51978677), Guangdong Basic and Applied Basic Research Foundation, China (2020A1515011271), and Shenzhen Natural Science Foundation (General Program), China (JCYJ20190807162401662). The authors are grateful to these institutions for their support.

References

[1] R. B. Peck, "Deep excavations and tunnelling in soft ground," in *Proceedings of 7th International Conference on Soil Mechanics and Foundation Engineering*, Mexico, 1969.

[2] H. J. Wu and G. Wei, "The calculation of soil settlement induced by construction of twin parallel shield tunnels with a small-interval," *Modern Tunnelling Technology*, vol. 51, no. 2, pp. 63–69, 2014.

[3] P. B. Attewell and M. R. Hurrell, "Settlement development caused by tunnelling in soil," *Ground Engineering*, vol. 18, no. 8, pp. 17–20, 1985.

[4] X. Xie, Y. Yang, and M. Ji, "Analysis of ground surface settlement induced by the construction of a large-diameter shield-driven tunnel in Shanghai, China," *Tunnelling and Underground Space Technology*, vol. 51, pp. 120–132, 2016.

[5] M. Sharifzadeh, F. Kolivand, M. Ghorbani, and S. Yasrobi, "Design of sequential excavation method for large span urban tunnels in soft ground-niayesh tunnel," *Tunnelling and Underground Space Technology*, vol. 35, pp. 178–188, 2013.

[6] N. A. Do, D. Dias, P. Oreste, and I. Djeran-Maigre, "Three-dimensional numerical simulation of a mechanized twin tunnels in soft ground," *Tunnelling and Underground Space Technology*, vol. 42, pp. 40–51, 2014.

[7] S. Miro, M. König, D. Hartmann, and T. Schanz, "A probabilistic analysis of subsoil parameters uncertainty impacts on tunnel-induced ground movements with a back-analysis study," *Computers and Geotechnics*, vol. 68, pp. 38–53, 2015.

[8] A. T. C. Goh, W. Zhang, Y. Zhang, Y. Xiao, and Y. Xiang, "Determination of earth pressure balance tunnel-related maximum surface settlement: a multivariate adaptive regression splines approach," *Bulletin of Engineering Geology and the Environment*, vol. 77, no. 2, pp. 489–500, 2018.

[9] G. Zheng, X. Yang, H. Zhou, Y. Du, J. Sun, and X. Yu, "A simplified prediction method for evaluating tunnel displacement induced by laterally adjacent excavations," *Computers and Geotechnics*, vol. 95, pp. 119–128, 2018.

[10] A. M. Marshall and R. J. Mair, "Tunneling beneath driven or jacked end-bearing piles in sand," *Canadian Geotechnical Journal*, vol. 48, no. 12, pp. 1757–1771, 2011.

[11] G. V. Mathew and B. M. Lehane, "Numerical back-analyses of greenfield settlement during tunnel boring," *Canadian Geotechnical Journal*, vol. 50, no. 2, pp. 145–152, 2012.

[12] N. Moussaei, M. H. Khosravi, and M. F. Hossaini, "Physical modeling of tunnel induced displacement in sandy grounds," *Tunnelling and Underground Space Technology*, vol. 90, pp. 19–27, 2019.

[13] Y. Xiang, H. Liu, W. Zhang, J. Chu, D. Zhou, and Y. Xiao, "Application of transparent soil model test and DEM simulation in study of tunnel failure mechanism," *Tunnelling and Underground Space Technology*, vol. 74, pp. 178–184, 2018.

[14] C. Sagaseta, "Analysis of undraind soil deformation due to ground loss," *Géotechnique*, vol. 37, no. 3, pp. 301–320, 1987.

[15] A. Verruijt and J. R. Booker, "Surface settlements due to deformation of a tunnel in an elastic half plane," *Géotechnique*, vol. 48, no. 5, pp. 709–713, 1998.

[16] N. Loganathan and H. G. Poulos, "Analytical prediction for tunneling-induced ground movements in clays," *Journal of Geotechnical and Geoenvironmental Engineering*, vol. 124, no. 9, pp. 846–856, 1998.

[17] J. S. Yang, B. C. Liu, and M. C. Wang, "Modeling of tunneling-induced ground surface movements using stochastic medium theory," *Tunnelling and Underground Space Technology*, vol. 19, no. 2, pp. 113–123, 2004.

[18] B. Zeng and D. Huang, "Soil deformation induced by Double-O-Tube shield tunneling with rolling based on stochastic medium theory," *Tunnelling and Underground Space Technology*, vol. 60, pp. 165–177, 2016.

[19] Z. Zhang, M. Huang, and M. Zhang, "Theoretical prediction of ground movements induced by tunnelling in multi-layered soils," *Tunnelling and Underground Space Technology*, vol. 26, no. 2, pp. 345–355, 2011.

[20] F. Pinto and A. J. Whittle, "Ground movements due to shallow tunnels in soft ground. I: analytical solutions," *Tunnelling and Underground Space Technology*, vol. 140, no. 4, pp. 1–17, Article ID 04013040, 2013.

[21] F. Wang, H. Lu, B. Gou, X. Han, Q. Zhang, and Y. Qin, "Modeling of shield-ground interaction using an adaptive relevance vector machine," *Applied Mathematical Modelling*, vol. 40, no. 9-10, pp. 5171–5182, 2016.

[22] H. N. Wang, G. S. Zeng, and M. J. Jiang, "Analytical stress and displacement around non-circular tunnels in semi-infinite ground," *Applied Mathematical Modelling*, vol. 63, pp. 303–328, 2018.

[23] F. Kong, D. Lu, X. Du, and C. Shen, "Elastic analytical solution of shallow tunnel owing to twin tunnelling based on a unified displacement function," *Applied Mathematical Modelling*, vol. 68, pp. 422–442, 2019.

[24] J. F. Zou, F. Wang, and A. Wei, "A semi-analytical solution for shallow tunnels with radius-iterative-approach in semi-infinite space," *Applied Mathematical Modelling*, vol. 73, pp. 285–302, 2019.

[25] B. Zeng, D. Huang, and J. He, "Analysis of Double-O-Tube shield tunnelling-induced soil deformation due to ground loss," *Géotechnique Letters*, vol. 6, no. 1, pp. 7–15, 2016.

[26] D. Huang and B. Zeng, "Influence of Double-O-tube shield rolling on soil deformation during tunneling," *International Journal of Geomechanics*, vol. 17, no. 11, Article ID 04017105, 2017.

[27] D. J. Ren, Y. S. Xu, J. Shen, A. Zhou, and A. Arulrajah, "Prediction of ground deformation during pipe-jacking considering multiple factors," *Applied Sciences*, vol. 8, no. 7, p. 1051, 2018.

[28] R. Liang, T. Xia, C. Lin et al., "Analysis of ground surface displacement and horizontal movement of deep soils induced by shield advancing," *Chinese Journal of Rock Mechanics & Engineering*, vol. 34, no. 3, pp. 583–593, 2015.

[29] C. Shi, C. Cao, and M. Lei, "An analysis of the ground deformation caused by shield tunnel construction combining an elastic half-space model and stochastic medium theory," *Ksce Journal of Civil Engineering*, vol. 21, no. 5, pp. 1933–1944, 2017.

[30] C. F. Wu, C. Wei, H. Y. Cao et al., "Analysis of lateral displacement of stratum caused by shield tunneling considering friction resistance of cutter head," *China Journal of Highway and Transport*, vol. 31, no. 10, pp. 201–213, 2018.

[31] G. Wei, X. Jiang, and X. Lin, "Research on additional load of adjacent underground pipelines caused by ground penetrating shield tunneling," *Chinese Journal of Underground Space and Engineering*, vol. 15, no. 1, pp. 232–239, 2019.

[32] W. Zhao, P. j. Jia, L. Zhu et al., "Analysis of the additional stress and ground settlement induced by the construction of Double-O-Tube shield tunnels in sandy soils," *Applied Sciences*, vol. 9, no. 7, p. 1399, 2019.

[33] Y. Zhu, L. Chen, H. Zhang, and T. Chen, "Quantitative analysis of soil displacement induced by ground loss and shield machine mechanical effect in metro tunnel construction," *Applied Sciences*, vol. 9, no. 15, p. 3028, 2019.

[34] P. Jia, W. Zhao, A. Khoshghalb et al., "A new model to predict ground surface settlement induced by jacked pipes with flanges," *Tunnelling and Underground Space Technology*, vol. 98, 2020.

[35] L. Y. Cheng, S. T. Ariaratnam, and S. X. Chen, "Analytical solution for predicting ground deformation associated with pipe jacking," *Journal of Pipeline Systems Engineering & Practice*, vol. 8, no. 3, 2017.

[36] R. D. Raymond, "Force at a point in the interior of a semi-infinite solid," *Physics*, vol. 7, no. 5, pp. 195–202, 1936.

[37] E. E. Alondso, A. Josa, and A. Ledesma, "Negative skin friction on piles: a simplified analysis and prediction procedure," *Géotechnique*, vol. 34, no. 3, pp. 341–357, 1984.